Plasma Chemistry and Plasma Processing, Vol. 1, No. 3, 1981

Two-Temperature Modeling of an Arc Plasma Reactor

D. M. Chen,[1] K. C. Hsu,[1] and E. Pfender[1]

Received March 17, 1981

In this paper a two-temperature plasma model is established and applied to the injection of cold gases into an atmospheric-pressure, high-intensity argon arc. The required nonequilibrium plasma composition and the non-equilibrium transport properties are also calculated. The results show that the arc becomes constricted at the location of gas injection due to thermal and fluid dynamic effects of the injected cold flow. Enhanced Joule heating in the constricted arc path raises the electron as well as the heavy-particle temperatures. This temperature increase resists, via secondary effects, the penetration of the cold gas into the hot arc core which behaves more or less as a "solid body" as far as the injected flow is concerned. The temperature discrepancy between electrons and heavy particles is most severe at the location of cold flow injection, a finding which may have important consequences on chemical reactions in an arc plasma reactor.

KEY WORDS: Arc plasma reactor; two-temperature modeling; nonequilibrium properties.

1. INTRODUCTION

This paper is concerned with the interaction of an atmospheric argon arc plasma confined in a long, water-cooled, cylindrical tube with a cold argon flow injected radially into the tube through a circumferential slit. This situation is typically experienced in the operation of arc-plasma reactors where gaseous reactants or particulate material is radially injected with a carrier gas flow.

In contrast to a previous study based on a single-temperature model,[(1)] this paper takes into account deviations from kinetic equilibrium. There is increasing evidence that the existence of local thermodynamic equilibrium (LTE) is rather the exception than the rule in so-called thermal plasmas.[(2)]

[1] Heat Transfer Division, Department of Mechanical Engineering, University of Minnesota, Minneapolis, Minnesota 55455.

0272-4324/81/0900-0295$03.00/0

The electron temperature T_e may be substantially higher than the heavy-particle temperature T close to walls and electrodes of high-intensity arcs as well as in the fringes of free-burning arcs.

Most of the previous experimental and analytical investigations of nonequilibrium arc plasmas have been concerned with the fully developed arc column confined in a water-cooled cylindrical tube in which radial convective velocities are negligible and temperature fields are independent of the axial coordinate.[3–8] Since the thermal and hydrodynamic flow fields are decoupled in this situation, the analysis of the arc column becomes a one-dimensional problem requiring, however, two coupled energy equations.

Relatively little effort has been devoted to the study of arc-flow interactions as experienced in plasma chemistry and plasma processing. The injection of particulate matter with a carrier gas flow plays, for example, an important role in plasma spraying, in plasma spheroidization, in plasma synthesis, in plasma reduction, and in plasma fuming. Progress in those growing fields is hampered by the poor understanding of arc-flow interactions, and the interaction of particulate matter with the plasma.

In this paper an attempt is made to clarify thermal and fluid dynamic effects of a radially injected flow on the arc plasma, based on a two-temperature model. The effects associated with particle injection will be reported elsewhere.

2. ANALYTICAL MODEL

Throughout this analysis the following assumptions will be used:

1. The arc is steady and rotationally symmetric and the flow is laminar.
2. Thermal diffusion effects are neglected.
3. Gravity and viscous heat dissipation are negligible.
4. The plasma is considered to be optically thin.
5. Only the self-magnetic field of the arc is considered (no external fields).
6. The electron gas and the heavy species are considered as two different perfect gases. Thermal equilibrium prevails among electrons and among heavy particles, but with different temperatures. The particle number densities are governed by the generalized mass action law.

Based on these assumptions, the conservation equations are expressed in terms of cylindrical coordinates (r, x, θ), where r is the radial distance, x the axial distance, and θ the angle.

Mass

$$\frac{\partial}{\partial x}(\rho u)+\frac{1}{r}\frac{\partial}{\partial r}(\rho r v)=0 \tag{1}$$

where ρ is the mass density, and u and v are the axial and radial velocity, respectively.

Momentum

$$\rho u\frac{\partial u}{\partial x}+\rho v\frac{\partial u}{\partial r}=-\frac{\partial p}{\partial x}+2\frac{\partial}{\partial x}\left(\mu\frac{\partial u}{\partial x}\right)+\frac{1}{r}\frac{\partial}{\partial r}\left(\mu r\frac{\partial u}{\partial r}\right)$$
$$+\frac{1}{r}\frac{\partial}{\partial r}\left(\mu r\frac{\partial v}{\partial x}\right)+j_r B_\theta \tag{2}$$

$$\rho u\frac{\partial v}{\partial x}+\rho v\frac{\partial v}{\partial r}=-\frac{\partial p}{\partial r}+\frac{\partial}{\partial x}\left(\mu\frac{\partial v}{\partial x}\right)+\frac{2}{r}\frac{\partial}{\partial r}\left(\mu r\frac{\partial v}{\partial r}\right)$$
$$+\frac{\partial}{\partial x}\left(\mu\frac{\partial u}{\partial r}\right)-\frac{2\mu v}{r^2}-j_x B_\theta \tag{3}$$

In these equations p, μ, j_r, j_x, and B_θ are the pressure, the viscosity, the radial and the axial current density, and the self-magnetic field, respectively.

Since $j_x \gg j_r$, the self-induced magnetic field B_θ may be written as

$$B_\theta=\frac{\mu_0}{r}\int_0^r j_x\xi\,d\xi \tag{4}$$

where μ_0 is the permeability of vacuum. Current continuity requires that

$$\frac{\partial j_x}{\partial x}+\frac{1}{r}\frac{\partial}{\partial r}(r j_r)=0 \tag{5}$$

or

$$\frac{\partial}{\partial x}\left(\sigma\frac{\partial\phi}{\partial x}\right)+\frac{1}{r}\frac{\partial}{\partial r}\left(\sigma r\frac{\partial\phi}{\partial r}\right)=0 \tag{6}$$

where σ is the electrical conductivity and ϕ is the electrical potential. The electron energy equation assumes the form

$$\frac{\partial}{\partial x}\left[\tfrac{5}{2}n_e k T_e u\right]+\frac{1}{r}\frac{\partial}{\partial r}r\left[\tfrac{5}{2}n_e k T_e v\right]$$
$$=\frac{5}{2}\frac{k}{e}\left[j_x\frac{\partial T_e}{\partial x}+j_r\frac{\partial T_e}{\partial r}\right]+\frac{\partial}{\partial x}\left(K_e\frac{\partial T_e}{\partial x}\right)+\frac{1}{r}\frac{\partial}{\partial r}\left(K_e r\frac{\partial T_e}{\partial r}\right)$$
$$+\frac{j_x^2+j_r^2}{\sigma}-S_R-\dot{E}_{eh} \tag{7}$$

where n_e is the electron density, k is the Boltzmann constant, e is the electron charge, T_e is the electron temperature, K_e is the thermal conductivity of the electrons, and S_R is the optically thin radiation term.

The energy-exchange term between electrons and heavy particles may be written as

$$\dot{E}_{eh} = \tfrac{3}{2}k(T_e - T)n_e\left(\frac{2m_e}{m_a}\right)\left(\frac{8kT_e}{\pi m_e}\right)^{1/2}(n_a Q_{ea} + n_i Q_{ei}) \tag{8}$$

where T is the heavy-particle temperature, m_e is the electron mass, m_a is the mass of the heavy species, n_a and n_i are the number of densities of the atoms and ions, respectively, and Q_{ea}, Q_{ei} are the collision cross sections of electron–atom and electron–ion collisions, respectively.

The left-hand side of Eq. (7) represents the mass convection of the electron enthalpy. The first term on the right-hand side stands for the transport of the electron enthalpy due to electron drift processes. The other terms in sequence are the electron conduction, Joule heating, and radiation loss.

The heavy-particle energy equation may be written as

$$\frac{\partial}{\partial x}[(\tfrac{5}{2}n_h kT + n_i\varepsilon_i)u] + \frac{1}{r}\frac{\partial}{\partial r}r[(\tfrac{5}{2}n_h kT + n_i\varepsilon_i)v]$$

$$= \frac{\partial}{\partial x}\left[K_{\text{eff}}\frac{\partial T}{\partial x}\right] + \frac{1}{r}\frac{\partial}{\partial r}\left[K_{\text{eff}}\, r\frac{\partial T}{\partial r}\right] + \dot{E}_{eh} \tag{9}$$

where n_h and n_i are the number densities of heavy particles and ions, respectively. The enthalpy of the heavy species includes the ionization energy ε_i. The quantity K_{eff} is the effective thermal conductivity, which is the sum of the translational thermal conductivity of the heavy species, K_h, and the reactive thermal conductivity, K_r. The electrons transfer energy to the heavy species by collisions and they pick up energy readily from the electric field due to their high mobility.

The arc configuration which is considered here is shown schematically in Fig. 1. The arc is confined in a relatively long, water-cooled constrictor tube with radius r_0. The working gas (argon) is introduced at the cathode end of the tube, and as it flows along the tube it picks up thermal energy from the arc, reaching a hydrodynamically and thermally fully developed state at the cross section AB, as indicated in Fig. 1. Within the fully developed regime of the arc, the plasma is subjected to a radial injection of argon at CD, through a circumferential slit which keeps the problem two-dimensional. At the location of cold gas injection, the arc is forced to contract owing to the associated strong cooling effect. Downstream of the injection slit, the arc plasma redevelops, i.e., the injected gas is gradually heated by the arc, reaching again a fully developed state at EF.

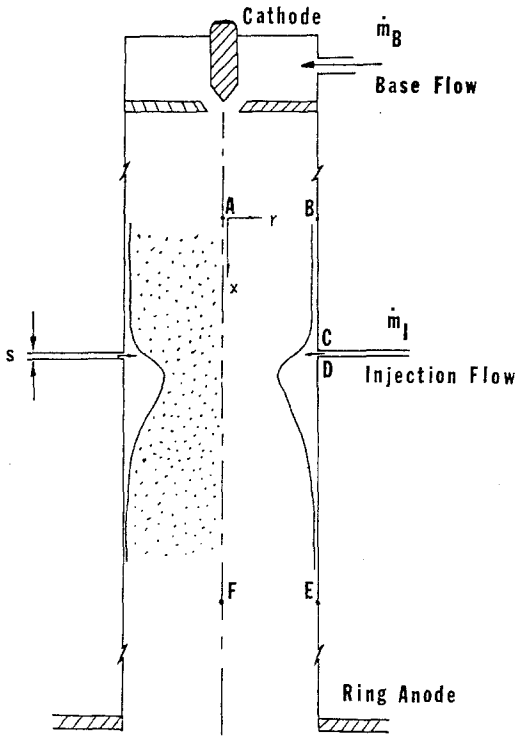

Fig. 1. Schematic diagram of the arc configuration and of the solution domain.

A solution domain *ABCDEFA* is specified as shown in Fig. 1 where a fully developed arc column exists both at *AB* and *EF*. Both locations are sufficiently far upstream or downstream from the injection slit. The boundary conditions used in this analysis are as follows:

On *AF*	On *AB*	On *BC* and *DE*	On *CD*	On *EF*
$v=0$	$v=0$	$v=0$	$v=v_{\text{inj}}$	$v=0$
$\frac{\partial u}{\partial r}=0$	$u=u_{\text{f.d}}$	$u=0$	$u=0$	$\frac{\partial u}{\partial x}=0$
$\frac{\partial T_e}{\partial r}=0$	$T_e=(T_e)_{\text{f.d}}$	$\frac{\partial T_e}{\partial r}=0$	$\frac{\partial T_e}{\partial r}=0$	$\frac{\partial T_e}{\partial x}=0$
$\frac{\partial T}{\partial r}=0$	$T=(T)_{\text{f.d}}$	$T=T_w$	$T=T_{\text{inj}}$	$\frac{\partial T}{\partial x}=0$
$j_r=0$	$j_x=\sigma E_{\text{f.d}}$	$j_r=0$	$j_r=0$	$j_r=0$

Along the centerline AF, the boundary conditions are obvious. Along the line AB, velocity, temperatures, and electric field strength are obtained from solutions of the fully developed arc column for a given total current (I) and a base mass flow rate ($\dot{m}_B$). On the tube wall, i.e., along BC and DE, no slip conditions for the velocity are postulated. In addition, there is no current flow into the constrictor tube. The temperature on the tube wall is assumed to be uniform. Specification of a realistic electron temperature close to the wall would have to rely on experimental data. It turns out, however, that the solutions converge rather quickly to an electron temperature of approximately 9000 K close to the wall regardless of the electron temperature assumed at the wall.[9] At the same time the slope of the electron temperature distribution approaches zero close to the wall. The latter finding suggests using the slope rather than the electron temperature itself as a boundary condition. This assumption is physically sound, because the wall is electrically insulated and the electron heat conduction into the wall becomes negligible. Therefore, $(\partial T_e/\partial r)_{\text{wall}} = 0$ is considered to be a realistic boundary condition. The injected flow enters the constrictor tube radially (i.e., $u = 0$). The radial injection velocity v is related to the given injection mass flow rate as $\dot{m}_I = \rho(2\pi r_0)sv$, where s is the width of the circular slit. The injection temperature at CD is assumed to be equal to the wall temperature because of the small dimension of the slit ($s = 1$ mm in this study). Along EF, the flow and temperature fields are again fully developed.

The previously discussed equations for a two-temperature plasma are solved with the stated boundary conditions by an iterative finite-difference scheme with a nonuniform grid system.[9] A total of 390 grid points (26 in the axial direction, 15 in the radial direction) are employed for the computations, corresponding to the maximum storage capacity available in the CDC 6400 computer for this complex system of coupled equations. Because of the anticipated steep gradients in the injection region, a rather fine grid (0.175 mm in the radial direction and 1 mm in the axial direction) is utilized for this region.

The solution of the conservation equations, however, requires knowledge of the plasma composition as a function of electron and heavy-particle temperatures and, in addition, the nonequilibrium transport coefficients must be known. The derivation of these quantities will be discussed below.

3. THE COMPOSITION OF A TWO-TEMPERATURE ARC PLASMA

For the case of singly ionized monatomic gases in which the excitation temperature due to electron collisions equals the electron temperature, the

generalized mass action law may be written as[10]

$$n_e\left(\frac{n_i}{n_a}\right)^{1/\theta} = \frac{g_e g_i(T_e)}{g_a(T_e)}\left(\frac{2\pi m_e k T_e}{h_c^2}\right)^{3/2} \exp\left(-\frac{\varepsilon_i - \Delta\varepsilon_i}{kT_e}\right) \tag{10}$$

where $\theta \equiv T_e/T$ is the ratio of electron to heavy-particle temperatures, $g_e = 2$ is the statistical weight of the electrons, g_i and g_a are the excitational partition functions of ions and atoms, respectively, h_c is Planck's constant, k is Boltzmann's constant, and $(\varepsilon_i - \Delta\varepsilon_i)$ is the lowered ionization potential. According to Griem,[11] the lowering of the ionization potential may be evaluated from

$$\Delta\varepsilon_i = \frac{ze^2}{4\pi\varepsilon_0\lambda_D} \tag{11}$$

where z is the electrical charge of the ions, for instance, $z = 1$ for n_i^+, $z = 2$ for n_i^{++}, etc., ε_0 is the dielectric constant, and e is the elementary charge of an electron. The Debye shielding length λ_D for the case under consideration takes the form[12]

$$\lambda_D = \left[\frac{\varepsilon_0 k T_e}{e^2 n_e(1+\theta)}\right]^{1/2} \tag{12}$$

With the model chosen for this analysis, each species can be considered to behave as a perfect gas, individually in thermal equilibrium with itself. The thermal equation of state of the mixture, i.e., Dalton's law, becomes

$$p = \sum_s p_s = \sum_s n_s k T_s \tag{13}$$

where p is the total pressure of the mixture. For a three-component, two-temperature arc plasma, Dalton's law may be written as (the ion temperature is assumed to be equal to the temperature of neutral atoms)

$$p = n_e k T_e + (n_i + n_a) kT \tag{14}$$

Quasi-neutrality with singly ionized species only requires that

$$n_e = n_i \tag{15}$$

Therefore, the composition of a three-component, two-temperature plasma can be determined from Eqs. (10), (14), and (15). The mass density may be obtained from

$$\rho = m_e n_e + m_a(n_i + n_a) \tag{16}$$

4. PLASMA TRANSPORT PROPERTIES

Although several theoretical computations of the transport properties for a thermal argon plasma are available in the literature, e.g., Ref. 13, there are relatively few papers concerned with the calculation of two-temperature properties.[14–16] Unfortunately, the usefulness of the data based on a two-temperature model is reduced due to a certain degree of uncertainty, and these data are not complete.

Since transport properties are a prerequisite for arc modeling, there is a pressing need for calculating nonequilibrium transport properties.

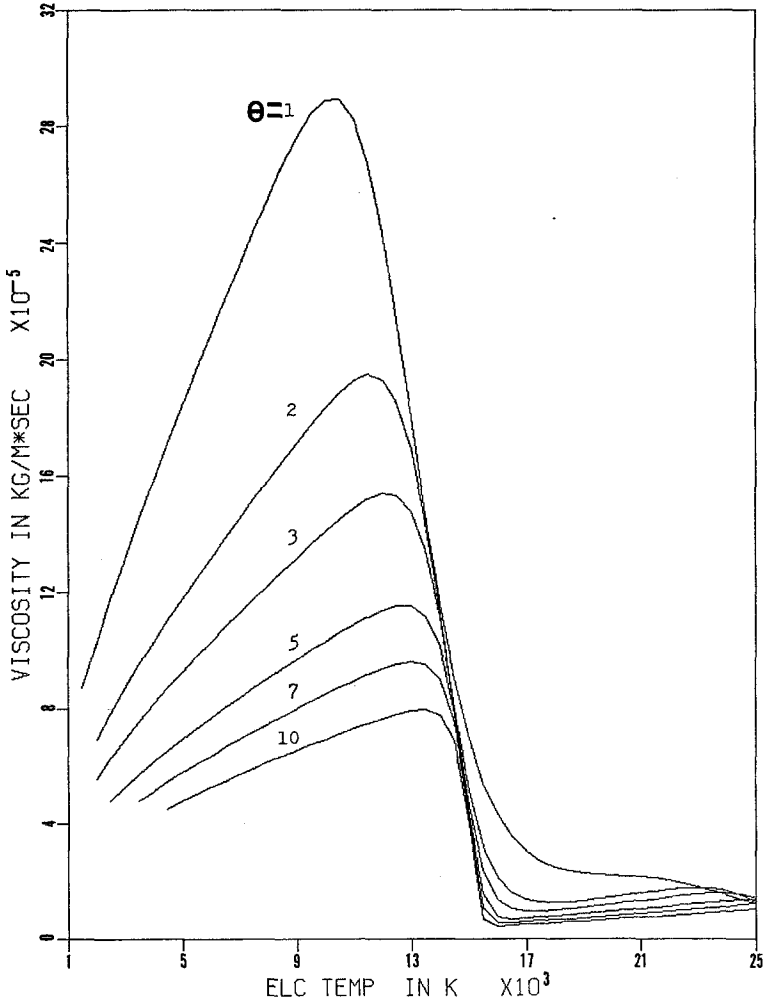

Fig. 2. Viscosity of a two-temperature argon plasma at $p = 1$ atm; $\theta = T_e/T$.

Computations of nonequilibriums transport properties of plasmas are essentially based on solutions of the Boltzmann integrodifferential equation. Because of the relatively small mass of the electron, the electrons may be decoupled from the Boltzmann equation of the heavy species. By using the Chapman–Enskog approach,[17] the transport coefficients of electrons and heavy species can be computed independently. This work has been recently completed,[18] part of whose results are used in the present analysis. Figures 2–4 show the viscosity, the electrical conductivity, and the total thermal conductivity ($K_T = K_e + K_h + K_r$), respectively.

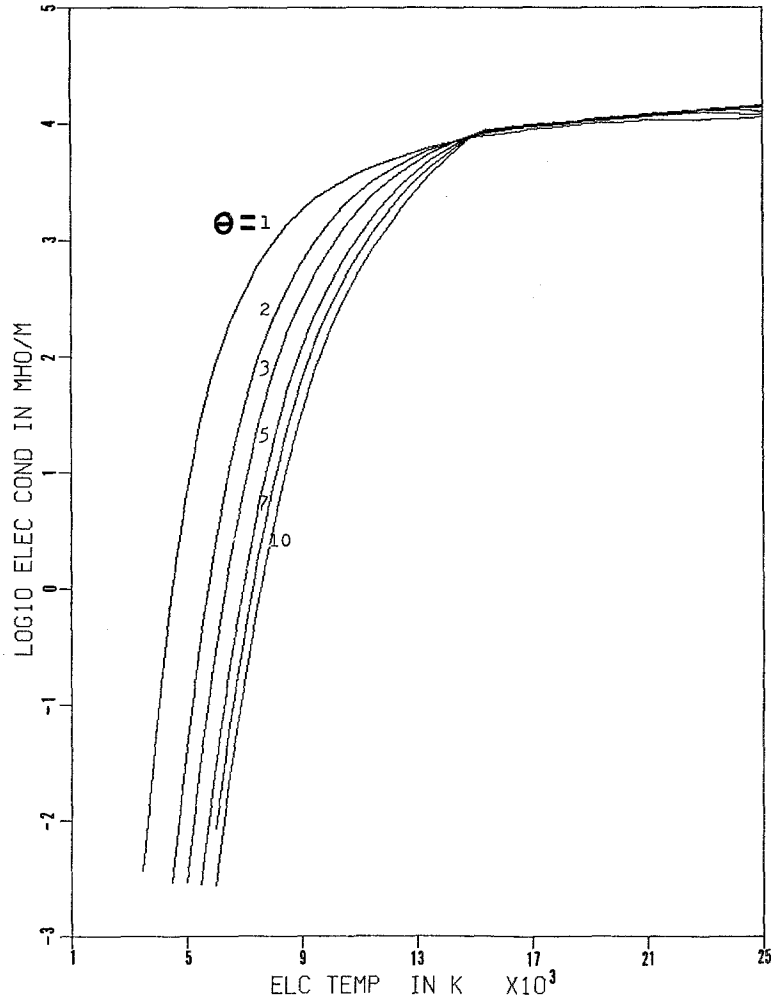

Fig. 3. Electrical conductivity of a two-temperature argon plasma at $p = 1$ atm; $\theta = T_e/T$.

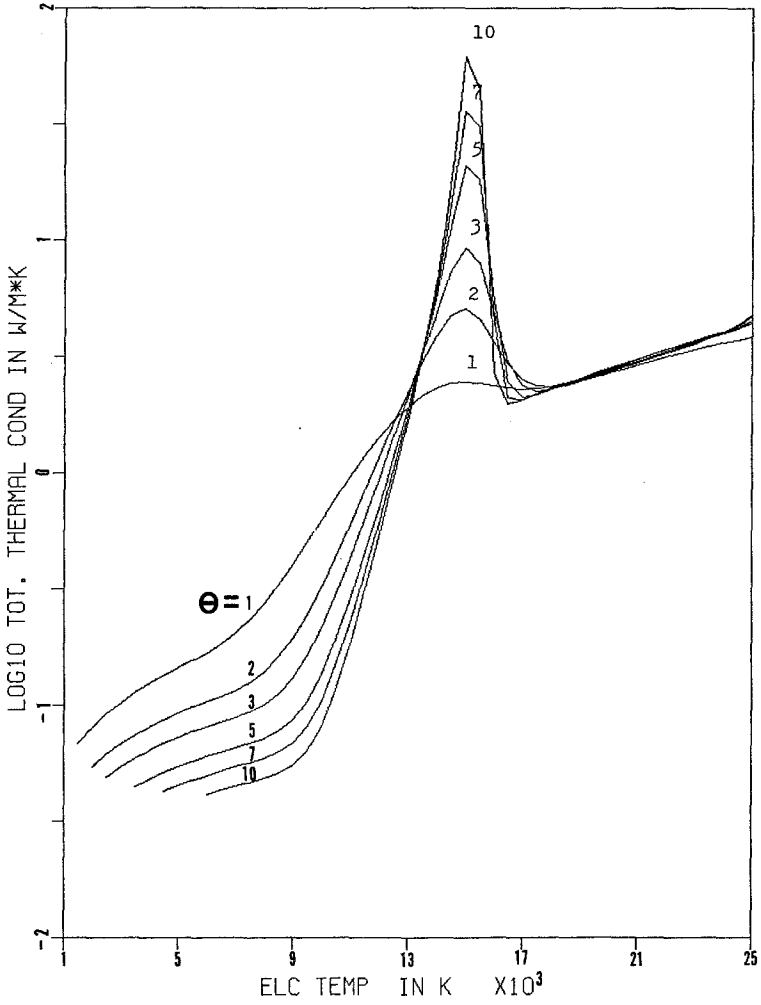

Fig. 4. Thermal conductivity of a two-temperature argon plasma at $p = 1$ atm; $\theta = T_e/T$.

5. NUMERICAL RESULTS AND DISCUSSION

The results refer to the following parameter range:

Arc current	$I = 200$ A
Base mass flow rate	$\dot{m}_B = 0.165$ g/s
Injection flow rate	$0.165 \leq \dot{m}_I \leq 0.495$ g/s
Temperature of constrictor tube	$T_w = 1000$ K
Temperature of injected gas	$T_{\text{inj}} = 1000$ K

Size of injection slit	$S = 1$ mm
Radius of constrictor tube	$r_0 = 5$ mm
Length of solution domain	$L = 10$ cm (line AF in Fig. 1)

First, results are shown for an atmospheric argon arc using an injection mass flow rate of $\dot{m}_I = 0.357$ g/s. If an injection ratio β is defined as $\dot{m}_I/\dot{m}_B$, then the aforementioned case corresponds to $\beta = 2.16$. The computations of the other cases with the same base mass flow rate but different values of the injection ratio β, namely 1.0 and 3.0, are meant to show the effects of the cold gas injection parameter on the behavior of the arc.

The isotherms of the electrons and of the heavy particles are shown in Figs. 5 and 6 where the dashed lines indicate the maximum penetration of the injected flow into the arc. It should be pointed out that the scales of radial and axial coordinates are different, i.e., the total radial distance is 5 mm while the total axial distance is 10 cm. Although the maximum penetration of the injection fluid is about half of the tube radius in this case, the thermal influence extends all the way into the arc core region. Owing to the cooling effect associated with the injected fluid, the arc

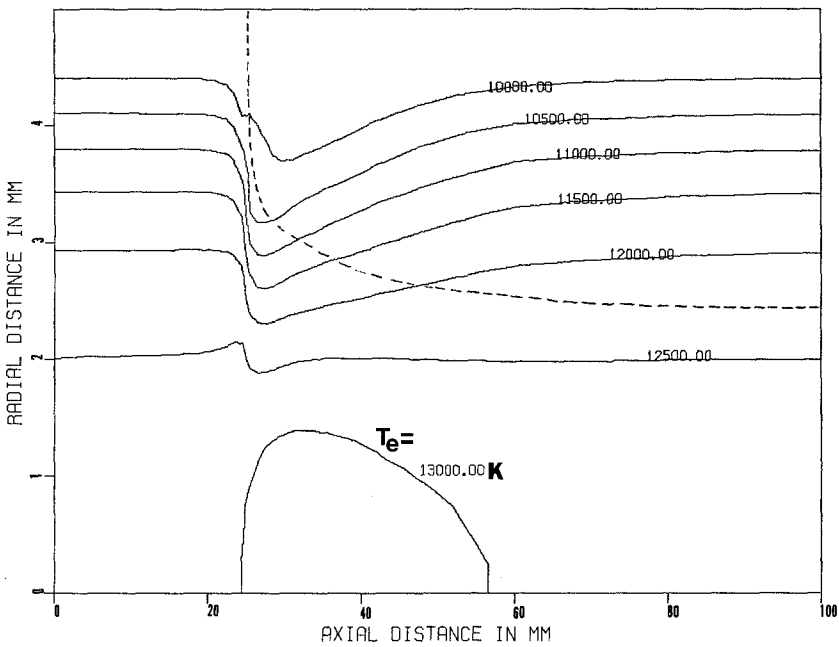

Fig. 5. Electron-temperature distribution in an argon arc at $p = 1$ atm, $I = 200$ A, and $s = 1$ mm. $\dot{m}_I = 0.357$ g/s and $\dot{m}_B = 0.165$ g/s for $\beta = 2.16$. The dashed curve is for maximum penetration of the injected flow.

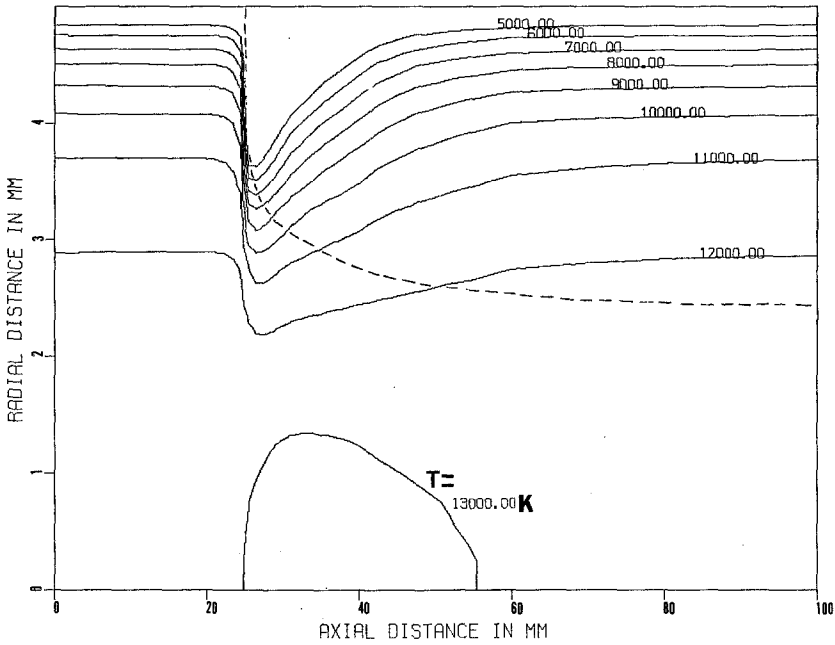

Fig. 6. Heavy-particle temperature distribution in an argon arc at $p = 1$ atm, $I = 200$ A, and $s = 1$ mm. $\dot{m}_I = 0.357$ g/s and $\dot{m}_B = 0.165$ g/s for $\beta = 2.16$. The dashed curve is for maximum penetration of the injected flow.

responds by an increase of both current density and electric field strength which enhances the local Joule heating, resulting in increased temperatures in the arc core. The temperature fields of electrons and heavy particles in the core region increase upstream as well as downstream of the injection slit. In general, electron and heavy-particle temperatures above 12,000 K are almost identical, which is the case in the arc core region. In the outer region near the injection slit, the electron temperature is substantially elevated over the heavy-particle temperature.

The flow field in terms of normalized streamlines is illustrated in Fig. 7. As expected, the base flow is squeezed at the location of gas injection and redevelops downstream of the injection slit. Over a relatively short distance, the injected gas is forced into the direction of the base flow. As can be seen in Fig. 7, the injected gas downstream of the injection slit is slightly repelled toward the tube wall due to the increased Joule heating in that region. This may at least partially explain why particulate matter is "rejected" by the arc.

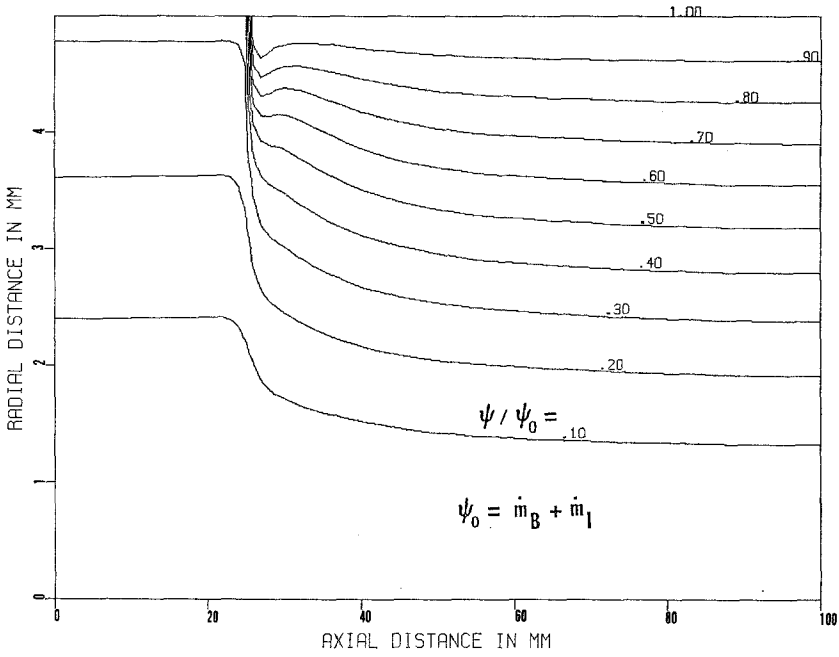

Fig. 7. Flow field in an argon arc at $p = 1$ atm, $I = 200$ A, and $s = 1$ mm. $\dot{m}_I = 0.357$ g/s and $\dot{m}_B = 0.165$ g/s for $\beta = 2.16$.

The radial distributions of electron and heavy-particle temperatures at different axial locations are presented in Fig. 8. The centerline of the injection slit is located at $x = 2.55$ cm. From this plot, it appears that the spatial extent of kinetic nonequilibrium increases at the location of fluid injection.

The distributions of radial velocity, temperature, radial momentum, and viscosity at the location of the injection slit are displayed in Fig. 9. In the direction from the tube wall toward the arc axis, the radial velocity is first diminished due to the increasing viscosity, followed by an unexpected acceleration of the flow which is, in part, due to the sharp decrease of the mass density and, in part, due to the pumping action caused by the imbalanced part of the $\mathbf{j} \times \mathbf{B}$ force in the overall momentum equation. This equation may be written as

$$\mathbf{j} \times \mathbf{B} = \text{grad}\, p + \rho \frac{d\mathbf{V}}{dt} \tag{17}$$

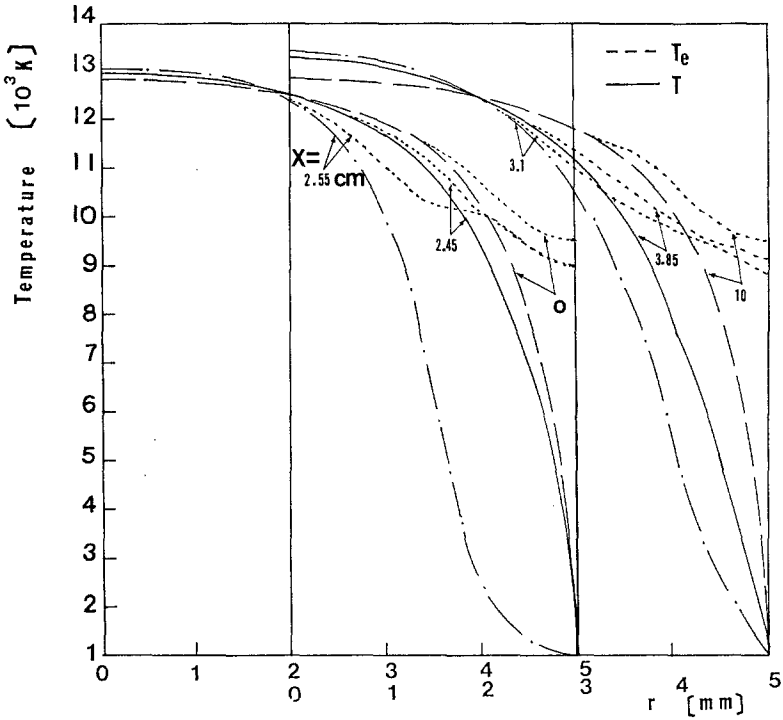

Fig. 8. Electron and heavy-particle temperature distributions at various axial locations in an argon arc at $p = 1$ atm, $I = 200$ A, and $s = 1$ mm. $\dot{m}_I = 0.357$ g/s and $\dot{m}_B = 0.165$ g/s for $\beta = 2.16$.

In an undisturbed, cylindrical arc column, the $\mathbf{j} \times \mathbf{B}$ force is balanced by the radial pressure gradient, i.e., $\rho \, d\mathbf{V}/dt = 0$. At the location of gas injection, however, the acceleration term exists, accelerating the gas toward the arc axis. This acceleration is, however, opposed by the still increasing viscosity. As the momentum of the injected flow decreases (Fig. 9), the momentum of the base flow forces the injected flow into the direction of the base flow. The relative strength of the momentum of injected flow and base flow finally determines the penetration of the injected flow into the arc.

The discrepancy between T_e and T is most severe in the arc fringes close to the wall. Figure 9 clearly shows that most of the injected mass stays in this region; only a small fraction penetrates further into the arc downstream from the injection slit (Figs. 5 and 6). This result may have important consequences for nonequilibrium plasma chemistry ($T_e > T$) at high gas densities.

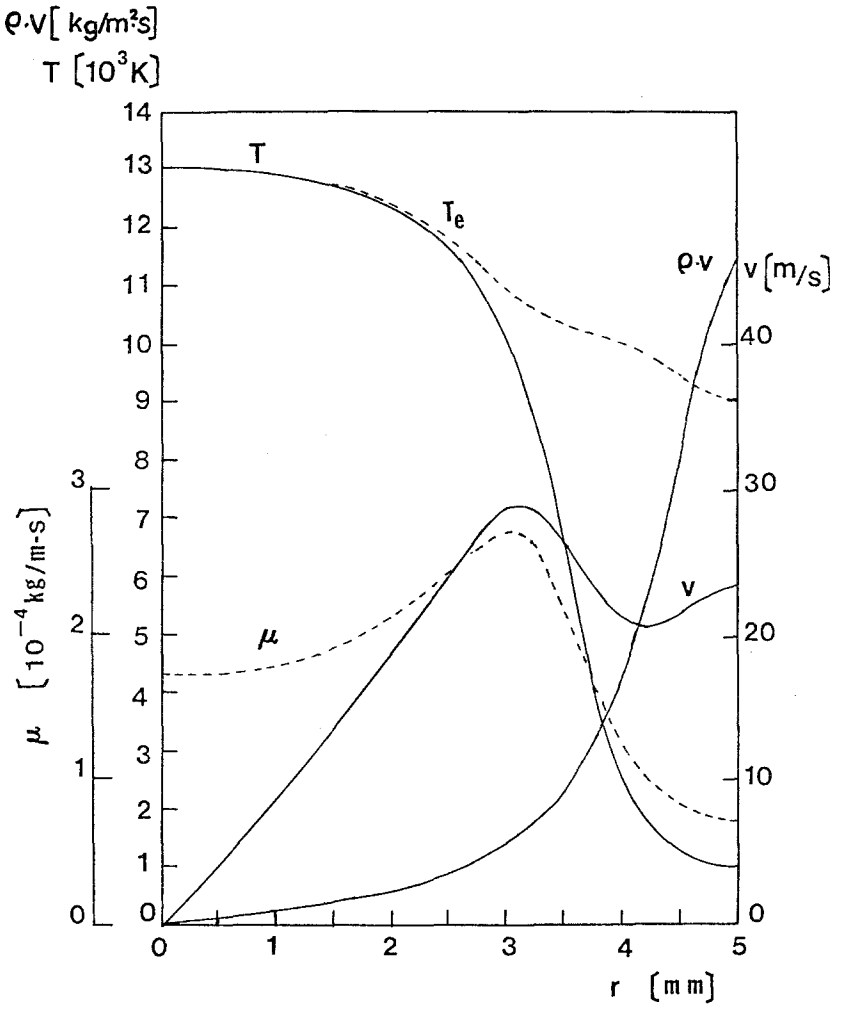

Fig. 9. Distribution of T, T_e, μ, v, and ρv in the injection plane of an argon arc at $p = 1$ atm, $I = 200$ A, and $s = 1$ mm. $\dot{m}_I = 0.357$ g/s and $\dot{m}_B = 0.165$ g/s for $\beta = 2.16$.

Similar sets of computed results for $\beta = 1.0$ and 3.0 reveal that the penetration of the injected flow and the resulting distortion of the temperature fields increase as the injection ratio increases. A recirculation bubble may be found slightly downstream of the injection slit. In general, this recirculation is only found for large values of β, and its size remains relatively small, confined to the region close to the wall.

The centerline velocity distributions are presented in Fig. 10 for different injection ratios. It is evident that the redeveloping length increases as the injection ratio increases. Figure 11 demonstrates the effect of different injection ratios on the centerline current density distributions. It is interesting to note that the current density starts already to increase upstream of the injection slit. In addition, the maximum values of the current density occur a few millimeters downstream from the injection slit.

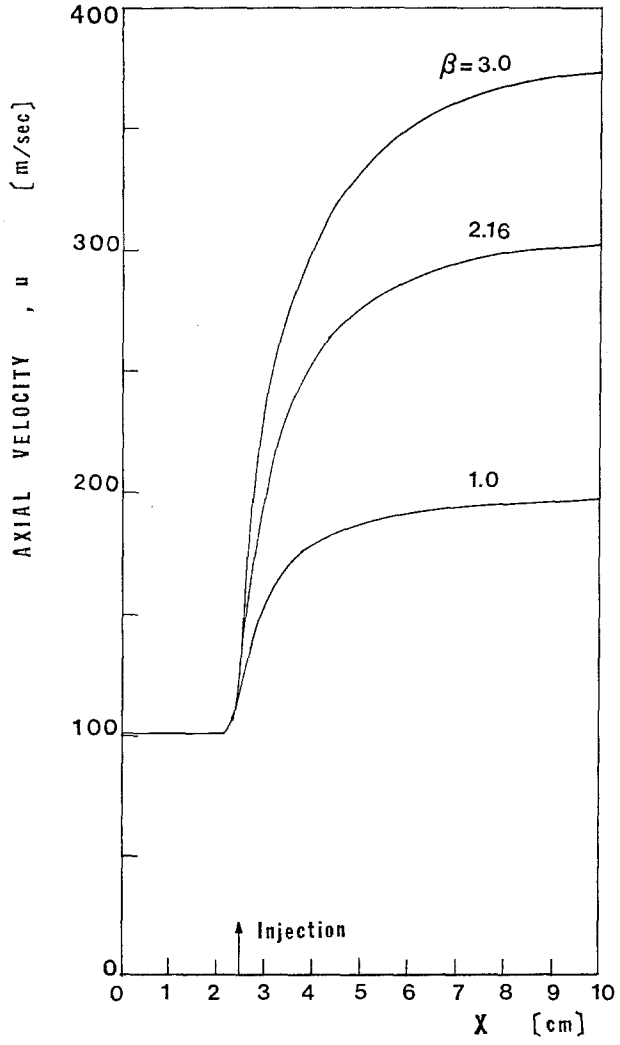

Fig. 10. Axial velocity distribution in an argon arc at $p = 1$ atm, $I = 200$ A, and $s = 1$ mm.

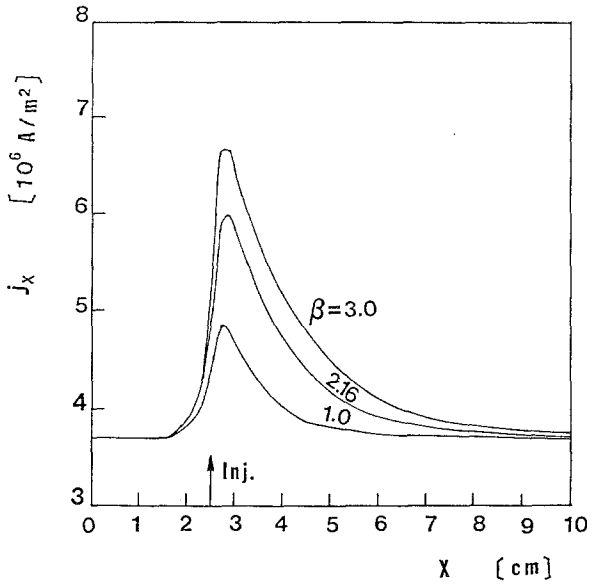

Fig. 11. Axial current density distribution in an argon arc at $p = 1$ atm, $I = 200$ A, and $s = 1$ mm.

Finally, the results of this study are summarized in Table I. Numbers in parentheses refer to results obtained for a one-temperature model under identical conditions. The maximum heat dissipation in the arc core increases with increasing injection ratio which is due to both the increase of the

Table I. Summary of Results[1]

	$\beta = \dot{m}_I/\dot{m}_B$		
	1.0	2.16	3.0
Max. $\dot{E}_{eh}$ (10^9 W/m^3)	3.67	5.13	6.00
Max. heat dissipation (10^9 W/m^3)	4.06 (5.19)	5.96 (8.55)	7.34
Max. current density (10^6 A/m^2)	4.87 (5.56)	6.01 (7.27)	6.73
Max. velocity (m/s)	197 (202)	301 (310)	373
Max. penetration (mm)	1.85 (1.86)	2.53 (2.50)	2.81
Flow redevelopment (mm)	16.0 (20.0)	25.0 (30.0)	30.0

[1] Values in parentheses refer to the one-temperature model.

current density and of the field strength. The maximum velocity as well as the maximum penetration increase with increasing injection ratio, but less than proportional. Also, these results are not sensitive to deviations from thermal equilibrium, in contrast to the maximum current density and the maximum heat dissipation which are higher for equilibrium than for non-equilibrium situations. The redevelopment length increases with increasing injection ratio and, consistent with the previous discussion, the required redevelopment length is larger for the case of equilibrium.

6. SUMMARY AND CONCLUSIONS

1. The computed results show that the confined arc column becomes constricted at the location of gas injection due to thermal and fluid dynamic effects associated with the injected cold flow. The arc responds to the constriction by an increase of both current density and electric field strength in the core region, which enhances the Joule heating. As a consequence, an increase of both electron temperature and heavy-particle temperature is found in the arc core, which resists, via secondary effects, the penetration of the cold flow into the arc.

2. As the injection flow loses momentum, it is forced into the direction of the base flow and redevelops downstream of the injection slit. The hot core of the arc acts almost as a solid body as far as the injected flow is concerned. As expected, the flow redevelopment length increases with increasing injection ratio. This length is 3 to 6 times the tube radius r_0 ($=5$ mm) for an atmospheric argon arc at $I = 200$ A, $\dot{m}_B = 0.165$ g/s, and $\beta = 1$ to 3.

3. The temperature discrepancy between electrons and heavy particles is most severe at the location of cold flow injection. At the same time the spatial extent of thermal nonequilibrium increases also due to the cooling effect associated with the injection flow. Although a small fraction of the injected gas is ingested by the arc downstream from the injection slit, the majority of this gas remains in the regime of severe nonequilibrium. This finding may have important consequences, particularly for plasma syntheses. Gaseous reactants injected into the arc will remain in the arc fringes, i.e., the desired chemical reactions may primarily occur in regions of elevated electron temperature. The same situation prevails if fine powders are injected into the arc either with an inert or with a chemically reacting carrier gas flow, since the fine particles will essentially follow the flow pattern of the carrier gas.

4. A comparison of results based on a one- and a two-temperature model for an undisturbed arc column (fully developed arc regions) is shown in Fig. 12. Since deviations from kinetic equilibrium occur primarily in the

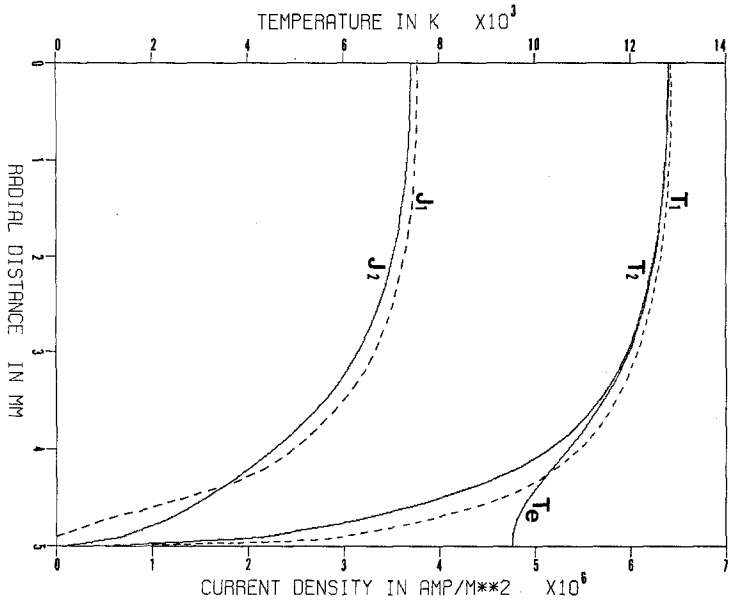

Fig. 12. Temperature and current density distribution in a fully developed argon arc at $p = 1$ atm and $I = 200$ A. T_1, J_1 refer to the one-temperature (LTE) model; T_e, T_2, J_2 refer to the two-temperature model.

arc fringes where the temperature drops below 12,000 K, the current density suffers also distortions in the arc fringes, as shown in Fig. 12. The two-temperature model provides a substantially higher electrical conductivity close to the wall and, as a consequence, the current density will also be higher close to the wall. This fact gives rise to a rearrangement of the entire current density distribution, although the effect on the arc core remains small.

ACKNOWLEDGMENTS

This work has been supported by the National Science Foundation under grant NSF/CPE 8008950.

REFERENCES

1. D. M. Chen, K. C. Hsu, C. H. Liu, and E. Pfender, The Effects of Cold Gas Injection on a Confined Arc Column, *IEEE Trans. Plasma Sci.* **PS-8**, No. 4, 425 (1980).
2. E. Pfender, Electric Arcs and Arc Gas Heaters, in *Gaseous Electronics*, Vol. 1, M. N. Hirsh and H. J. Oskam, eds. (Academic Press, New York, 1978), p. 291.

3. A. Pytte and N. K. Winsor, A Two-Temperature Theory for a Helium Arc Plasma in a Cylindrical Duct, *Proc. Int. Conf. Phenom. Ionized Gases*, 7th, Beograd, Vol. 1 (1965), p. 709.
4. C. H. Kruger, Non-equilibrium in Confined-Arc Plasmas, *Phys. Fluids* **13**, No. 7, 1737 (1970).
5. K. J. Clark and F. P. Incropera, Thermochemical Non-equilibrium in an Argon Constricted Arc Plasma, AIAA Paper No. 71-593; *AIAA J* **10**, No. 1, 17 (1972).
6. A. A. Voropaev and S. V. Dresvin, Two-Temperature Model of a Laminar Arc under Conditions of Forced Blowing of Gas through a Plasmatron, *Teplofiz. Vys. Temp.* **11**, No. 2, 333 (1973).
7. F. P. Incropera, Procedures for Modeling Laminar Cascade Arc Behavior, *IEEE Trans. Plasma Sci.* **PS-1**, No. 3, 3 (1973).
8. R. K. Scott and F. P. Incropera, Non-equilibrium Flow Calculations for the Hydrogen Constricted Arc, *AIAA J.* **11**, No. 12, 1714 (1973).
9. D. M. Chen, Analytical Modeling of Two-Temperature Argon Arc Plasmas, Ph.D. Thesis, University of Minnesota (1980).
10. A. V. Potapov, Chemical Equilibrium of Multitemperature Systems, *High Temp.* **4**, No. 1, 48 (1966).
11. H. R. Griem, *Plasma Spectroscopy* (McGraw-Hill, New York, 1964).
12. S. Veis, The Saha Equation and Lowering of the Ionization Energy for a Two-Temperature Plasma, *AIAA Tech. Inform. Serv.* No. A68-44609.
13. R. S. Devoto, Transport Coefficients of Ionized Argon, *Phys. Fluids* **16**, No. 5, 616 (1973).
14. D. Kannappan and T. K. Bose, Transport Properties of a Two-Temperature Argon Plasma, *Phys. Fluids* **20**, No. 10, 1668 (1977).
15. E. J. Miller and S. I. Sandler, Transport Properties of Two-Temperature Partially Ionized Argon, *Phys. Fluids* **16**, No. 4, 491 (1973).
16. U. Daybelge, Transport Properties of Two-Temperature Partially Ionized Plasmas, Ph.D. Thesis, Stanford University (1968).
17. J. O. Hirschfelder, C. F. Curtiss and R. B. Bird, *Molecular Theory of Gases and Liquids* (Wiley, New York, 1964).
18. K. C. Hsu and E. Pfender, Calculation of Thermodynamic and Transport Properties of a Two-Temperature Argon Plasma, Proceedings of the Fifth Internat. Symp. on Plasma Chemistry, Vol. 1, 144 (1981); Heriot-Watt Univ., Edinburgh, Scotland.